First-principles computation of elasticity of $Pb(Zr,Ti)O_3$: The importance of elasticity in piezoelectrics

R.E. Cohen*, E. Heifets* and H. Fu†

*California Institute of Technology, Pasadena, CA and Carnegie Institution of Washington, 5251 Broad Branch Rd., N.W., Washington, D.C. 20015
†Department of Physics, Rutgers University, Camden, NJ 08102

Abstract. We have computed the elastic constant tensor for $PbZrTiO_6$, PZT 50/50, in the rhombohedral structure. We find it to be very soft elastically, and the Young's modulus to be very anisotropic. Our results for PZT are compared with literature values on other oxide perovskites, and the new experimental results on PMN-PT and PZN-PT. The elastic response is an important part of the electromechanical response, and should be studied experimentally and theoretically to help build up a systemic understanding of electromechanical materials. We find that anisotropy in Young's modulus and elastic softness may be key discriminators in evaluating or improving electromechanical properties.

INTRODUCTION

We now understand the origin of ferroelectricity in perovskite oxide ferroelectrics. Ferroelectricity results from a delicate balance of long-range and short-range forces [1–3]. The long-range forces destabilize the cubic structure, and are enhanced generally by large transverse effective charges. The large effective charges are largely the result of hybridization between the O 2p states and the B-cation d-states, which are the lowest conduction band states. Short-range overlap forces stabilize the cubic structure, and hybridization helps soften these forces so that the ions can move off-center. The electromechanical response is a result of (a) the change in polarization with strain, which depends on the effective charges and the soft-mode potential surface [4–6], (b) the elastic constants, and (c) the dielectric tensors [7, 8]. First-principles studies of effective charges and hybridization in a number of systems now show no systematics that might indicate simply which compositions will have the strongest electromechanical coupling constants [6, 9–11]. In fact, effective charges (and local structure)in perovskite oxides vary little for a given ion for different bulk compositions; e.g. Ti in $PbTiO_3$ and in PZT are very similar [6]. Here we investigate the importance of elasticity in varying the effective coupling strengths of different piezoelectrics.

A knowledge of all aspects of the electromechanical coupling in piezoelectrics would be highly desirable to optimize materials and devices for applications. Surprisingly, even for the classic ferroelectrics such as $BaTiO_3$, apparently the single crystal tensors have not been measured for each of the piezoelectric phases, that is the rhombohedral, orthorhombic, and tetragonal phases. The situation for materials such as

CP582, *Fundamental Physics of Ferroelectrics 2001,* edited by H. Krakauer

$Pb(Zr,Ti)O_3$ (PZT) are even more problematic, since no single crystal data exist. Fortunately, single crystal data are being measured [12] for the new high-strain piezoelectrics $Pb(Mg,Nb)O_3$-$PbTiO_3$ (PMN-PT) and $Pb(Zn,Nb)O_3$-$PbTiO_3$ (PZN-PT) [13–15], and the new tentative results will be compared with our computations for PZT and other phases here.

For PZT, phenomenological models fit to ceramic and powdered data have been successful to systematize data, but it is not clear that they have predictive power. For example, a major recent discovery of a monoclinic phase at the morphotropic phase boundary near compositions of 52/48 PZT [16, 17] was not anticipated by such models, probably because the underlying sixth order Devonshire theory could not encompass a monoclinic phase [18]. In spite of the fact that PZT can now be grown in small crystals of 10-20 microns, which are large enough for Brillouin scattering studies to extract single crystal elastic and piezoelectric constants, no such data exist. First-principles methods have been used to study the zero temperature piezoelectric strain coefficients e_{ij} in $PbTiO_3$ and e_{33} in 50/50 PZT. The temperature dependence of the piezoelectric stress coefficients d_{ij} have been studied in [8, 19–21] using model Hamiltonians fit to first-principles calculations. However, there apparently have been no studies of elasticity in ferroelectric perovskites. Here we compute the full set of single crystal elastic constants for ordered PZT 50/50 in the rhombohedral structure.

A most important parameter for piezoelectric applications, including acoustic transducers and actuators is the electromechanical coupling coefficient, k_{ij} [22]. The ratio of stored energy to input energy is given by k^2 and

$$k^2 = \frac{d^2}{\varepsilon s} \tag{1}$$

where ε is the dielectric constant tensor and s is the compliance tensor. The piezoelectric strain tensor is

$$d_{ijk} = \frac{\partial \varepsilon_{ij}}{\partial E_k} \tag{2}$$

$$P_i = d_{ijk}\sigma_{jk} \tag{3}$$

where ε is the strain, σ is the stress, E is the applied electric field and P is the polarization. The elastic compliance tensor is

$$s_{ijkl} = \frac{\partial \sigma_{ij}}{\partial \varepsilon_{kl}} \tag{4}$$

Although d_{ijk} can be determined straightforwardly from an effective Hamiltonian, it is more straightforward to compute the piezoelectric stress coefficients

$$e_{ijk} = \frac{\partial P_i}{\partial \varepsilon_{jk}} \tag{5}$$

$$P_i = e_{ijk}\varepsilon_{jk} \tag{6}$$

in self-consistent calculations, since electronic structure computations in periodic boundary conditions are always formally performed at constant $E = 0$ (although one

can introduce a small potential perturbation that mimics an electric field). The polarization P_i can be computed from first-principles using the Berry's phase theory for polarization in bulk solids [23, 24]. By computing the polarization versus applied strains, one can compute the piezoelectric stress coefficients. These two different piezoelectric tensors are related through the elastic compliances $d_{ijk} = e_{ilm}s_{lmjk}$.

The piezoelectric, stress, strain, elastic, and compliance tensors indices are usually contracted as $11 \rightarrow 1$, $22 \rightarrow 2$, $33 \rightarrow 3$, $32 \rightarrow 4$, $13 \rightarrow 5$, $12 \rightarrow 6$, so that stresses and strains are represented by one index, and piezoelectric, elastic and compliance tensors by two indices. (See Nye [25] for details of numerical factors in some cases.) In Voigt notation, the elastic constants and compliance are represented as matrices, and are the inverse of each other.

In previous studies, we have computed the piezoelectric stress tensor for $PbTiO_3$ and the e_{33} constant for PZT 50/50 in the tetragonal structure [5, 6, 11]. Although the results for $PbTiO_3$ were in good agreement with experiment, e_{33} for PZT was of similar magnitude, and seemed too small using ceramic data for elastic compliances to estimate e_{33} for ceramics.

Whereas piezoelectricity was considered largely as a collinear effect, with the strain, electric field, and polarization in parallel, computations for polarization rotation, with the polarization direction rotated from (111) to (001) with a field along (001) showed very large piezoelectric response, consistent with the new large strain piezoelectrics.[26, 27] This effect is also consistent with the large piezoelectric coupling seen near the morphotropic phase boundary between rhombohedral and tetragonal phases in PZT, with the discovery of a monoclinic phase in this region, apparently at zero field.[28, 29] The monoclinic phase can be understood as an intermediate state between the rhombohedral (polarization 111) and tetragonal (polarization 001) phases. The large coupling in such PZT's can be thought of as a self-induced polarization rotation, as opposed to the field induced rotation in the large strain single crystals PMN-PT and PZN-PT. This effect also occurs in PZT's away from the monoclinic phase.

The question remains how much of the strong coupling is due directly to the anisotropy and softness of the elasticity, and how much is due to the underlying polarization rotation energy surface? Here we compute the elastic constants for ordered PZT 50/50 in a rhombohedral structure and examine the effects of elastic softening and anisotropy. Ordering has not been experimentally detected in PZT, and the 50/50 composition falls in the tetragonal phase field. We study the rhombohedral structure since it has the larger piezoelectric response, and is the "parent structure" of the monoclinic phase and the large coupling single crystal piezoelectrics. The use of an ordered structure is an approximation, and our results can be used as a benchmark to compare with faster, "second-principles" methods that can be used to study disordered systems.

METHOD

We have computed the energy versus strain for ordered PZT to obtain the elastic constants. We used the local density approximation and a mixed basis pseudopotential method [30]. The basis consists of the pseudoorbitals and a small number of plane

TABLE 1. Lattice and positions of atoms in zero strain (minimum energy) structure with $a = 5.78626$ Åand $\alpha = 59.2445°$ ($V = 134.63$ Å^3/10 atoms). The positions are given in terms of the lattice vectors.

lattice vectors (Å):			
	-2.86003	-1.65123	4.75126
	2.86003	-1.65123	4.75126
	0.00000	3.30247	4.75126
atomic positions:			
Pb(1)	-0.00476	-0.00476	-0.00476
Pb(2)	0.49313	0.49313	0.49313
Ti	0.26212	0.26212	0.26212
Zr	0.76231	0.76231	0.76231
O(1)	0.03100	0.03100	0.53012
O(2)	0.53012	0.03100	0.03100
O(3)	0.03100	0.53012	0.03100
O(4)	0.04493	0.51550	0.51550
O(5)	0.51550	0.04493	0.51550
O(6)	0.51550	0.51550	0.04493

waves. The pseudoorbitals, as well as the charge density and potential are expanded as plane waves, to a large cut-off wavevector G_{max}. The basis set size is much smaller, consisting of 9 orbitals per atom, plus plane waves up to a small g_{max}. The pseudopotential is a Troullier-Martins type [31] with r_{match}= 1.70, 2.00, and 1.75 bohr for $6s^1$, $6p^1$, and $5d^{10}$ for Pb, 1.50, 1.60, 1.75 bohr for $4s^2$, $4p^6$, and $4d^{0.5}$ for Zr, 1.45, 1.40, and 1.75 for $3s^2$, $3p^6$, and $3d^{0.5}$ for Ti, and 1.5, 1.5, and 2.5 for $2s^2$, $2p^4$, and $3d^{0.2}$ for O. The small g_{max} was 120 eV and the large cut-off G_{max} was 884 eV. Since the basis can be expanded in plane waves, all integrals can be computed using FFT methods. One can consider the pseudoorbitals to be contractions of large numbers of plane waves, and convergence is obtained with a relatively small basis.

The Zr and Ti ions were ordered like the rock-salt structure on the B sites. The reference structure (zero strain) was obtained by relaxing the atomic positions and rhombohedral strain in the ten atom supercell, at the experimental volume of 134.63 Å^3 [32]. The rhombohedral strain is small, the minimum energy rhombohedral angle (with relaxed atomic positions) is 59.2445°, as opposed to 60° for the fcc cubic lattice, and a=5.78626 Å. Table 1 shows the atomic positions for the unstrained structure.

There are six independent elastic constants for the rhombohedral group 3m: C_{11}, C_{33}, C_{12}, C_{13}, C_{14}, and C_{44}. Six different strains were applied to the reference structure, and the atomic positions were relaxed using analytic forces and a conjugate gradient algorithm. Table 2 shows the strains used and the linear combinations of elastic constants for each strain, and table 3 shows the elastic constants in terms of the second derivatives of the energy with respect to each strain. Note that zero strain refers to the experimental volume and the minimum energy rhombohedral strain. Internal degrees of freedom were relaxed for each strain. Figure 1 shows the energy versus strain for each case.

TABLE 2. Strains used to determine elastic constants and the second order change in energy.

	strain	Δ E
$e_1 = \varepsilon_3$	$\varepsilon_{11} = \varepsilon_{22} = -\frac{1}{2}\varepsilon_{33} = \varepsilon_3$	$(\frac{1}{4}(C_{11}+C_{12}) - C_{13} + \frac{1}{2}C_{33})\varepsilon_3^2$
$e_2 = \varepsilon_3$	$\varepsilon_{11} = \varepsilon_{22} = \varepsilon_{33} = \varepsilon_3$	$(C_{11}+C_{12}+2C_{13}+\frac{1}{2}C_{33})\varepsilon_3^2$
$e_3 = \varepsilon_4$	$2\varepsilon_{23} = \varepsilon_4$	$\frac{1}{2}C_{44}\varepsilon_4^2$
$e_4 = \varepsilon_6$	$2\varepsilon_{12} = \varepsilon_6$	$\frac{1}{2}(C_{11}-C_{12})\varepsilon_6^2$
$e_5 = \varepsilon_6$	$2\varepsilon_{12} = 2\varepsilon_{13} = \varepsilon_6$	$(C_{14}+\frac{1}{2}C_{44}+\frac{1}{4}(C_{11}-C_{12}))\varepsilon_6^2$
$e_6 = \varepsilon_3$	$\varepsilon_{33} = \varepsilon_3$	$\frac{1}{2}C_{33}\varepsilon_3^2$

RESULTS AND DISCUSSION

The energy versus strain was fit to a fourth order polynomial for each case, and the coefficient of the quadratic term derived (the B's in Table 3, and resulting elastic constants and compliances are shown in Table 4.

Note the extreme softness of the C_{44} modulus compared with the others. This is also

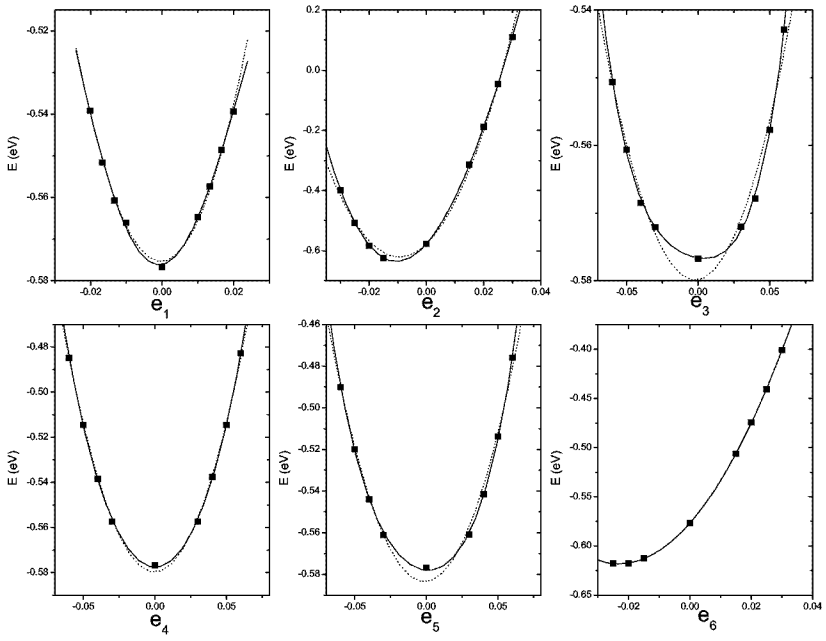

FIGURE 1. Energy versus strain for each set of strains. Strains correspond to those in Table 2. Dashed lines are from second order fits, and solid lines are fourth order fits.

TABLE 3. Elastic constants in terms of B_i, the second derivatives of the energy versus the strains e_i from table 2.

C_{11}	$(2B_1+B_2+6B_4-3B_6)/6$
C_{33}	B_6
C_{12}	$(2B_1+B_2-6B_4-3B_6)/6$
C_{13}	$(-4B_1+B_2+3B_6)/12$
C_{14}	$(-B_3-B_4+B_5)/2$
C_{44}	B_3

TABLE 4. Elastic constants (GPa) and compliances ($1000\,\mathrm{GPa}^{-1}$). Also shown is the bulk modulus and compressibility. The C's are the coefficients for the strain-energy density. The c's are for the stress-strain relations, such that the stress in the strained state T is given by $T_{\alpha\beta} = \sigma_{\alpha\beta} + c_{\alpha\beta\sigma\tau}\varepsilon_{\sigma\tau} + \sigma_{\beta\tau}\omega_{\alpha\tau} + \sigma_{\alpha\tau}\omega_{\beta\tau}$, where σ is the stress in the reference state ("unstrained"), ε is the symmetric strain relative to the reference state, and ω is the rotation (antisymmetric strain) from the reference state. The compliances are given for the stress-strain relation (c's).

C_{11}	235	c_{11}	235	s_{11}	6.75
C_{33}	180	c_{33}	180	s_{33}	6.13
C_{12}	126	c_{12}	122	s_{12}	-3.67
C_{13}	58.5	c_{13}	54.1	s_{13}	-0.93
C_{14}	-9.5	c_{14}	-9.5	s_{14}	9.4
C_{44}	8.4	c_{44}	10.5	s_{44}	111.9
K	123				

the strain that couples most strongly with the soft-modes, and is very anharmonic as can be seen in Figure 1.

Since the stress is not zero at the reference configuration, it is necessary to distinguish between the elastic constants obtained from the energy expansion (3) and those for stress versus strain [33]. The relationship between the two for hydrostatic pressures is:

$$\begin{aligned} c_{11} &= C_{11} \\ c_{33} &= C_{33} \\ c_{12} &= C_{12}+P \\ c_{13} &= C_{13}+P \\ c_{14} &= C_{14} \\ c_{44} &= C_{44}-\frac{1}{2}P \end{aligned} \tag{7}$$

where P is -4.3 GPa in our case.

We now consider various averages for application to ceramics and thin films. The elastic response of a polycrystal or ceramic depends on the texture and orientations of the crystallites [34]. The simplest, most general bounds are the Voigt bound, which assumes uniform strain, and the Reuss bound, which assumes uniform stresses. In the elastic

TABLE 5. Average bulk and shear moduli (GPa) for randomly oriented aggregates. Results are compared with experimental values for ceramic PZT 50/50 [35], and recent tentative results for PMN-33% PT and PZN-8% PT [12]. Voigt is the upper bound, Reuss the lower bound, and Hill the average estimate.

	Theory PZT	Exp. PZT	PMN-33% PT	PZN-8% PT
Voigt:				
bulk	123		112	103
shear	43		43	39
Reuss:				
bulk	117		105	101
shear	18		11	8
Hill:				
bulk	120	76	108	102
shear	31	30	27	24

TABLE 6. Comparison of computed PZT bulk modulus with experiments on other oxide perovskites [35–40].

	K (GPa)
PZT 50/50	123 (this study), 76 (exp.)
$CaTiO_3$	212, 179
$BaTiO_3$	196, 156, 139
$SrTiO_3$	179, 172
$PbTiO_3$	204
$PbZrO_3$	102
PMN-33% PT	112
PZN-8% PT	103

limit in mechanical equilibrium under load (for example in a well annealed sample under stress), the strain should approach that of the Reuss limit. The acoustic response is usually close to an average of the Reuss and Voigt limits, called the Hill estimate. We do not consider the variational Hashin-Strickman bounds here, which are narrower. The bounds are compared with experimental data on ceramic PZT 50/50 (which is probably tetragonal) in Table 5. The Hill estimate is very close for the shear modulus, but the experimental bulk modulus is significantly lower, perhaps due to porosity in the sample and/or LDA error. Actually values even for bulk moduli are hard to come by, so it is not clear if there is a problem with the theory or experiments for the bulk modulus. What is very clear though is that the large coupling materials, PZT 50/50, PMN-33% PT and PZN-8% PT are elastically very soft compared with other perovskite oxides, and the endmember compounds $PbTiO_3$ and $PbZrO_3$ (Table 6). In fact, the new experimental data on PMN-33% PT and PZN-8% PT [12] are very close to an elastic instability, which is also reflected in the large differences in the bounds for the average shear moduli, and their low values.

An important directionally dependent parameter for electromechanical applications is the Young's modulus, which gives the effective elastic constant for extension in one

direction and the spontaneous strains in other directions under constant stress. We have computed these surfaces for PZT and for comparison, for $BaTiO_3$ and $PbTiO_3$ (Fig. 2). Young's modulus is soft in more directions than for the other materials. Young's modulus varies from about 20 to 163 GPa in PZT, and from 64 to 216, and 30 to 220 GPa in tetragonal $BaTiO_3$ and $PbTiO_3$, respectively. PZT appears to be generally softer than other oxide perovskites, and this is clearly one contribution to the larger strains obtainable under applied fields. We cannot separate the contributions from soft mode coupling and homogeneous and other modes coupled with strain. It is clear, however, that the soft mode coupling plays a major role, since the strain i=3 (which gives C_{44}) corresponds to flexing the rhombohedral angle, and couples strongly with the soft mode. This can be seen from the large change in the second derivative for a homogeneous strain, compared with the internal contributions from relaxation of the atomic positions (not shown).

We have also considered some different averages of Young's modulus, (a) corresponding to cubic c-axes parallel to (001), but randomly oriented around this axis, (b) multidomain single crystals with cubic c-axes parallel to (001), and local polarization along one of the ($\pm 1 \pm 11$) directions, (c) randomly oriented grains in a poled sample, with polarization pointing along the (111) direction closest to the average polarization direction and (Fig. 3). The shape of the anisotropy varies strongly with the texture, represented by the different averaging schemes. Note also that the total anisotropy decreases significantly with averaging, which may be one reason that oriented single crystal piezoelectrics tend

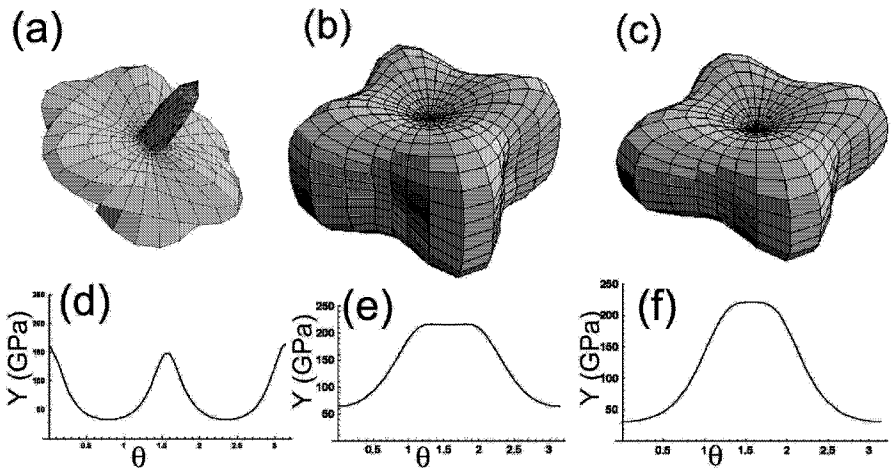

FIGURE 2. (a,d) Computed Young's modulus for rhombohedral PZT 50/50. The top figure (a) is a 3d spherical representation, with the length of the radius vector from the origin equal to the Young's modulus in that direction. The lower figure (d) shows Young's modulus as a function of direction for angles varying from the rhombohedral c-axis (cubic 111), $\theta = 0$, through the cubic (001), $\theta = 0.9553$, and around. (b,e) Experimental [38] Young's modulus for tetragonal $BaTiO_3$. (c,f) Experimental [41] Young's modulus for tetragonal $PbTiO_3$. For (e) and (f), $\theta = 0$ is the cubic (001) axis. The section along [110] is shown. PZT is much more anisotropic (and softer) than oxide perovskites.

to have much stronger coupling than poled ceramics.

We have also computed the Young's moduli for the new tentative data of Cao and Shrout [12] (Fig. 4), which are for a multidomain rhombohedral crystal. Note that it is extremely anisotropic and similar in many ways to the computed rhombohedral PZT 50/50 results, except the averaging apparently is different than our constant stress assumption. The large anisotropy in Young's modulus in these materials can be understood from the importance of polarization rotation. The (111) direction parallel to the polarization is the only direction for a Young's modulus strain that does not allow polarization rotation. The extreme anisotropy in PZN-8% PT and PMN-33% PT is a direct result of the softness for polarization rotation and the large coupling between polarization rotation and strain. Note that the bulk moduli are also soft, so that these material are soft elastically in all ways, not just with respect to shear. The PZT, PZT-PT, and PMN-PT compositions studied are all close to morphotropic phase boundaries. This is probably a key factor in the softening of the potential surface with respect to rotations. $BaTiO_3$ is also close to a phase transition, and PbTiO3 moderately so, but in their cases the response is not so anisotropic, and the rotational potential surface is stiffer, as was also seen in self-consistent total energy calculations for $BaTiO_3$[27].

Since elasticity and other electromechanical tensors of perovskites are often considered for the cubic cell, we have rotated our elastic constants to obtain the equivalent

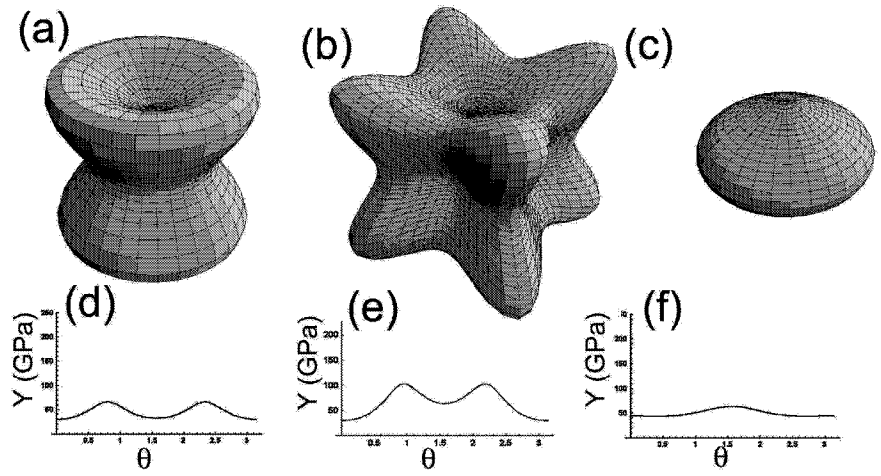

FIGURE 3. Computed Young's moduli for rhombohedral PZT 50/50 for several types of aggregates. (a,d) Rotational average around cubic (001) axis. This average is appropriate for a film or ceramic with c-axes perpendicular to the slab, and randomly oriented around this axis. See caption for fig. 2 for more details. (b,e) Multi-domain, single crystal average with cubic (001) axis vertical. This average assumes equal proportions of the four rhombohedral orientations ($\pm 1 \pm 11$) with net polarization along (001). (c,f) This average assumes random grain orientations, but for a poled sample with net polarization vertical. The assumption is that the polarization of each grain is along the rhombohedral c direction closest to the cubic (001) axis. For (e),(f), and (g) $\theta = 0$ is the cubic (001) axis. Note that the magnitude of Young's modulus is greatly decreased by the averaging process, compared with a single crystal. Also, the nature of the anisotropy is strongly dependent on the assumed texture.

TABLE 7. Computed PZT 50/50 elastic constant matrix (GPa) rotated to the cubic coordinate system.

145	112	112	3	-22	-22
112	145	112	-22	3	-22
112	112	145	-22	-22	3
3	-22	-22	61	11	11
-22	3	-22	11	61	11
-22	-22	3	11	11	61

elastic constants for the cubic axis system (Table 7). Note that the usual cubic symmetry is not present, since in fact the crystal is not cubic, but rhombohedral. Also, note that the strong anisotropy, so evident in the rhombohedral coordinate system with c along the cubic diagonal (111) direction, is hidden with c along the cubic (001) direction. The rotated constants are significantly different from the values extracted from ceramic data [35]. For example, the latter gives 111 GPa for C_{33} and 56 GPa for C_{13}, compared with 145 and 112 from Table 7. This illustrates that the elastic response of a poled ceramic cannot be considered in any way equivalent to the single crystal response. However, by modeling the texture and elastic response, it should be possible to predict ceramic behavior from the single crystal constants.

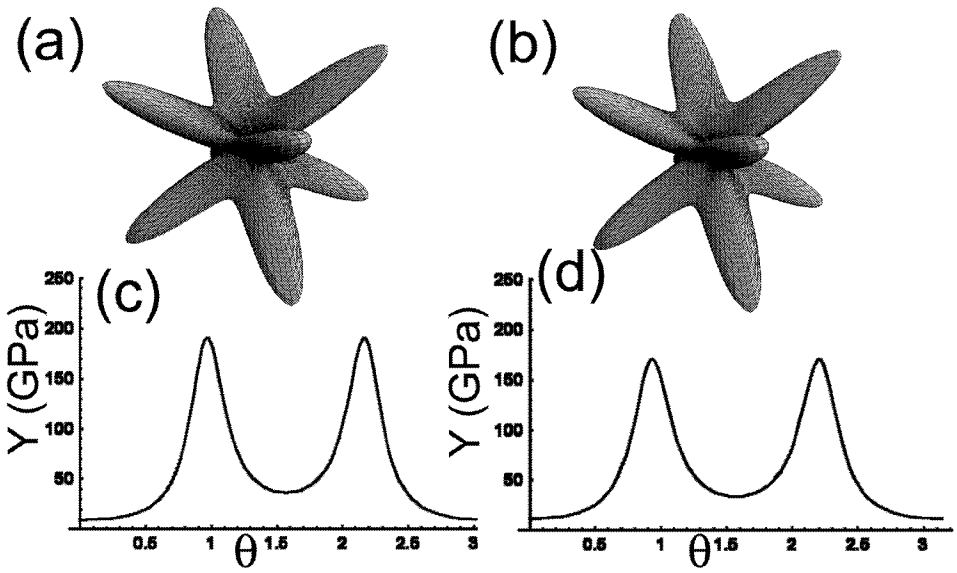

FIGURE 4. Computed Young's moduli for the tentative data [12] on (a,c) PZN-8% PT and (b,d) PMN-33% PT. The data are presented with tetragonal symmetry due to sample domains. For (c) and (d) $\theta = 0$ is the cubic (001) axis.

TABLE 8. Transformation matrix U for rotation of elastic constants in contracted Voigt notation to the cubic coordinate system.

$\frac{1}{2}$	$\frac{1}{2}$	0	0	0	$-\frac{1}{2}$
$\frac{1}{6}$	$\frac{1}{6}$	$\frac{2}{3}$	$-\frac{1}{3}$	$-\frac{1}{3}$	$\frac{1}{6}$
$\frac{1}{3}$	$\frac{1}{3}$	$\frac{1}{3}$	$\frac{1}{3}$	$\frac{1}{3}$	$\frac{1}{3}$
$\frac{\sqrt{2}}{3}$	$\frac{\sqrt{2}}{3}$	$-\frac{2\sqrt{2}}{3}$	$-\frac{1}{3\sqrt{2}}$	$-\frac{1}{3\sqrt{2}}$	$\frac{\sqrt{2}}{3}$
$\sqrt{\frac{2}{3}}$	$-\sqrt{\frac{2}{3}}$	0	$-\frac{1}{\sqrt{6}}$	$\frac{1}{\sqrt{6}}$	0
$\frac{1}{\sqrt{3}}$	$-\frac{1}{\sqrt{3}}$	0	$\frac{1}{\sqrt{3}}$	$-\frac{1}{\sqrt{3}}$	0

Since the transformation from rhombohedral to cubic coordinates will often be required as more data and theoretical elasticity computations for perovskites become available, we include for convenience the transformation U from c along the three-fold axis (cubic 111) to c along the cubic four-fold axis (cubic 001) for a fourth order tensor in Voigt notation (8). The transformation is applied as

$$C' = U^T C U. \tag{8}$$

The transformation is not orthogonal, and is equivalent to rotating the fourth rank tensor.

CONCLUSIONS

We have computed the elastic constant tensor for rhombohedral 50/50 PZT. We find that PZT is much softer elastically than other comparable oxide piezoelectrics. We find a similar picture in the new tentative data for PZN-8% PT and PMN-33% PT [12]. The high strain materials all have extreme anisotropy in the Young's modulus, and are soft in may directions. Understanding the elastic response is one of the key elements to designing better materials and using them to their best advantage in devices. These results also suggest that elasticity may be a screening diagnostic for looking for new materials and material improvements.

ACKNOWLEDGMENTS

This work was supported by the Office of Naval Research contract number N000149710052. We thank W. Cao and T. Shrout for allowing us to include their new data on PMN-PT and PZN-PT. Computations were performed on the Cray SV1 at the Geophysical Laboratory, supported by NSF EAR-9975753 and the Keck Foundation.

REFERENCES

1. Cohen, R. E., *Nature*, **358**, 136–138 (1992).
2. Cohen, R. E., and Krakauer, H., *Phys. Rev. B*, **42**, 6416–6423 (1990).
3. Cohen, R. E., and Krakauer, H., *Ferroelec.*, **136**, 65–84 (1992).
4. Bellaiche, L., and Vanderbilt, D., *Phys. Rev. Lett.*, **83**, 1347–1350 (1999).
5. Saghi-Szabo, G., Cohen, R. E., and Krakauer, H., *Phys. Rev. Lett.*, **80**, 4321–4324 (1998).
6. Saghi-Szabo, G., Cohen, R. E., and Krakauer, H., *Phys. Rev. B*, **59**, 12771–12776 (1999).
7. Bellaiche, L., and Vanderbilt, D., *Phys. Rev. B*, **61**, 7877–7882 (2000).
8. Rabe, K. M., and Cockayne, E., in *First-principles Calculations for Ferroelectrics: Fifth Williamsburg Workshop*, edited by R. E. Cohen, AIP, 1998, vol. 436, pp. 61–70.
9. Ghosez, P., Cockayne, E., Waghmare, U. V., and Rabe, K. M., *Phys. Rev. B*, **60**, 836–843 (1999).
10. Ghosez, P., Michenaud, J. P., and Gonze, X., *Phys. Rev. B*, **58**, 6224–6240 (1998).
11. Saghi-Szabo, G., Cohen, R. E., and Krakauer, H., in *First-Principles Calculations for Ferroelectrics: Fifth Williamsburg Workshop*, edited by R. E. Cohen, AIP, New York, 1998, vol. Conference Proceedings 436, pp. 43–52.
12. Cao, W., and Shrout, T. R., Personal communication (2001), unpublished.
13. Park, S. E., and Shrout, T. R., *Mat. Res. Innov.*, **1**, 20–25 (1997).
14. Park, S.-E., and Shrout, T. R., *J. Appl. Phys.*, **82**, 1804–1811 (1997).
15. Liu, S.-F., Park, S.-E., Shrout, T. R., and Cross, L. E., *J. Appl. Phys.*, **85**, 2810–2814 (1999).
16. Noheda, B., Cox, D., Shirane, G., Gonzalo, J., Cross, L., and Park, S., *Appl. Phys. Lett.*, **74**, 2059–2061 (1999).
17. Noheda, B., Gonzalo, J., Cross, L., Guo, R., Park, S., Cox, D., and Shirane, G., *Phys. Rev. B*, **61**, 8687–8695 (2000).
18. Vanderbilt, D., and Cohen, M. H., *Phys. Rev. B*, **63**, 94108–94117 (2001).
19. Bellaiche, L., Garcia, A., and Vanderbilt, D., *Phys. Rev. Lett.*, **84**, 5427–5430 (2000).
20. Cockayne, E., and Rabe, K. M., *Phys. Rev. B*, **57**, R13973–R13976 (1998).
21. Garcia, A., and Vanderbilt, D., *Appl. Phys. Lett.*, **72**, 2981–2983 (1998).
22. Uchino, K., *Acta Material.*, **46**, 3745–3753 (1998).
23. King-Smith, R. D., and Vanderbilt, D., *Phys. Rev. B*, **47**, 1651–1654 (1993).
24. Resta, R., *Rev. Mod. Phys.*, **66**, 899–915 (1994).
25. Nye, J. F., *Physical Properties of Crystals: Their Representation by Tensors and Matrices*, Oxford University Press, New York, 1985.
26. Fu, H., and Cohen, R. E., in *Fundamental Physics of Ferroelectrics 2000*, edited by R. E. Cohen, AIP, New York, 2000, vol. Conference Proceedings.
27. Fu, H., and Cohen, R. E., *Nature*, **403**, 281–283 (2000).
28. Du, X., Zheng, J., Belegundu, U., and Uchino, K., *Appl. Phys. Lett.*, **72**, 2421–2423 (1998).
29. Guo, R., Cross, L. E., Park, S., Noheda, B., Cox, D., and Shirane, G., *Phys. Rev. Lett.*, **84**, 5423–5426 (2000).
30. Gulseren, O., Bird, D. M., and Humphreys, S. E., *Surf. Sci.*, **402-404**, 827–830 (1998).
31. Troullier, N., and Martins, J.-L., *Phys. Rev. B*, **43**, 1993–2006 (1991).
32. Jaffe, H., Roth, R. S., and Marzullo, S., *J. Res. Nat. Bur. Stand.*, **55**, 239 (1955).
33. Barron, T. H. K., and Klein, M. L., *Proc. Phys. Soc.*, **85**, 523–532 (1965).
34. Anderson, O. L., *Equations of State of Solids for Geophysicists and Ceramic Science*, Oxford University Press, New York, 1995.
35. Berlincourt, D. A., Cmolik, C., and Jaffe, H., *Proceedings of the IRE*, **48**, 220–229 (1960).
36. Xiong, D. H., Ming, L., and Manghnani, M. H., *Phys. Earth Planet. Inter.*, **43**, 244 (1986).
37. Fischer, G. J., Wang, W. C., and Karato, S., *Phys. Chem. Minerals*, **20**, 97 (1993).
38. Berlincourt, D. A., and Jaffe, H., *Phys. Rev.*, **111**, 143 (1958).
39. Edwards, L. R., and Lynch, R. W., *J. Phys. Chem. Sol.*, **31**, 573 (1970).
40. Kobayashi, Y., Endo, S., Ming, L. C., Deguchi, K., Ashida, T., and Fujishita, H., *J. Phys. Chem. Sol.*, **60**, 57–64 (1999).
41. Gavrilyachenko, V. G., and Fesenko, E. G., *Soviet Phys. Cryst.*, **16**, 549 (1971).